Research Article | Vol. 29, No. 23 / 8 Nov 2021 / Optics Express 38109
Optics EXPRESS

Droplet microfluidic generation of a million optical microparticle barcodes

PAUL H. DANNENBERG,[1,2,4] JIE WANG,[1,3,4] YUE ZHUO,[1] SANGYEON CHO,[1] KWON-HYEON KIM,[1] AND SEOK-HYUN YUN[1,2,*]

[1]*Harvard Medical School and Wellman Center for Photomedicine, Massachusetts General Hospital, Boston, Massachusetts 02114, USA*
[2]*Harvard-MIT Health Sciences and Technology, Massachusetts Institute of Technology, Cambridge, Massachusetts 02139, USA*
[3]*College of Artificial Intelligence, Nanjing Agricultural University, Nanjing 210031, China*
[4]*Co-first authors with equal contribution.*
[*]*syun@hms.harvard.edu*

Abstract: Micron-scale barcode particles enable labelling of small objects. Here, we demonstrate high-throughput barcode fabrication inside a microfluidic chip that can embed multiple, dye-doped high quality-factor whispering gallery mode cavities inside aqueous droplets at kilohertz rates. These droplets are then cured to form polyacrylamide hydrogel beads as small as 30 μm in diameter. Optical resonance spectra of the embedded cavities provide the hydrogels with unique barcodes with their diversity combinatorically scaled with the number of embedded cavities. Using 3 cavities per hydrogel, we obtain approximately one million uniquely identifiable, optically readable barcode microparticles.

1. Introduction

Barcodes are a universal presence in everyday life where they are used to track items such as shop inventories. Much work has been expended in the development of barcodes that can fulfill a similar function at the microscale, enabling large numbers of different analytes to be simultaneously tagged, identified, and tracked across a series of analysis platforms. Applications using microparticle barcodes have been demonstrated in the formation of combinatorial chemical libraries [1], as indicators to identify pathogens [2], oligonucleotides [3], antibodies [4], and as cryptographic microtaggants [5].

One common approach to barcoding involves the creation of microparticles consisting of uniquely identifiable shapes [1,6] or spatial patterns [7,8] fabricated using lithographic techniques. This presents difficulties when used in three-dimensional environments in which the orientation of barcode is arbitrary. For example, deciphering imprinted micropatterns resembling Quick Response (QR) codes [8] is far from straightforward when tilted at oblique angles. Similarly, shape-based schemes [1,9] usually rely on a planar orientation to be correctly identified.

Another common barcoding strategy is to use optical emission such as fluorescence, which can be detected in all directions. For example, in a multiplexed immunoassay commercialized by Luminex [10], up to 500 types of fluorescent dye-doped microbeads of different colors and brightness are each coupled to different capture antibodies, which enables simultaneous screening of the different antibody targets using the bead color and intensity as a barcode to indicate the specific target being analyzed. However, the number of available unique microbead barcodes is still ultimately limited and not readily scalable due to spectral overlap between the different fluorescent dyes.

This limitation in fluorescence-based barcoding can be potentially overcome by generating barcodes based on the spectral signature of the resonance of light within the bead itself. A high refractive index bead can act as an optical cavity, trapping light emitted by the fluorophores. This

#439143 https://doi.org/10.1364/OE.439143
Journal © 2021 Received 2 Aug 2021; revised 5 Sep 2021; accepted 6 Sep 2021; published 1 Nov 2021

Optics EXPRESS

leads to the formation of sharp lines in each bead's emission spectrum, corresponding to the whispering gallery mode (WGM) resonances determined by the diameter of each bead [11,12]. However, previous studies using this form of spectral signature remain limited in multiplexing ability, with no more than 2,000 unique barcodes demonstrated [13,14].

Here, we demonstrate a new, highly scalable spectral barcoding scheme and the generation of such barcodes at the microscale using droplet microfluidics. By using a microfluidic platform, we are able to fabricate the barcodes at high-speed using a simple low-cost technique, with a low volume of starting material. These advantages render microfluidic platforms well-suited to the generation of microscale photonic devices which has led to their use in numerous prior studies [15–19]. Our optical barcodes consist of hydrogel microbeads (30-50 μm diameter) containing multiple fluorescently-doped microsphere cavities of random diameter (Fig. 1(a)), each of which supports WGM resonances (Fig. 1(b)). Unlike previous studies [13,14,20–22] in which barcodes are derived from the WGM of a single resonator, our technique generates barcode particles at kilohertz rates with multiple resonators embedded, hence termed multiplet particles. We are therefore able to generate a composite barcode, based on the resonances of each microsphere. Since these resonances are fundamentally determined by diameter, the barcode of a multiplet is described by a set of diameters of the constituent microspheres. Importantly, this strategy also allows us to generate approximately 10^6 unique, microscale optically readable barcodes.

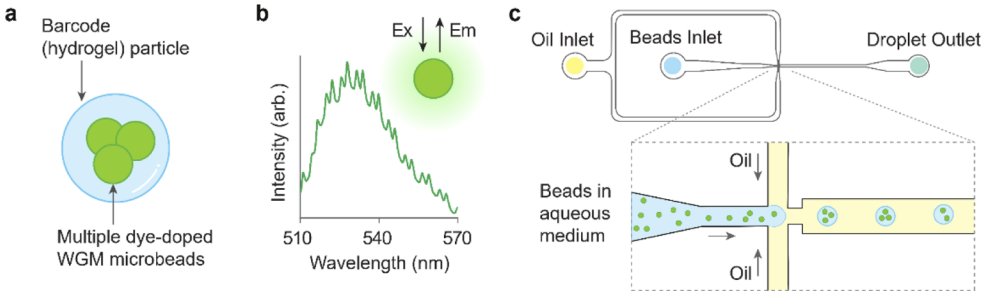

Fig. 1. Fabrication of barcode particles. (a) Constituents of the barcode particle. (b) Representative WGM spectrum from a single microsphere. (c) Schematic of microfluidic device (top) and illustration of the flow focusing junction (bottom).

2. Materials and methods

2.1. Microfluidic barcode production

Barcode particles were created using poly(dimethylsiloxane) (PDMS) microfluidic devices similar to previous literature designs [23,24]. The master-mold was fabricated using standard soft lithography techniques. SU-8 3050 (Kayaku Advanced Materials, Inc., Westborough, MA) was spun onto a silicon wafer (UniversityWafer Inc., Boston, MA) and patterned to define rectangular features that molded 50 μm high channels in the 10:1 base elastomer:curing agent PDMS. Inlet and outlet holes were punched in the device using a 1.2 mm diameter biopsy punch, enabling a snug fit for 1/16" OD (0.006" ID) PTFE tubing (Valco Instruments Co. Inc. Houston, TX). The PDMS was then bonded to a glass slide substrate by O_2 plasma bonding (Plasma Etch, Inc., Carson City, NV) (30 s, 30 W, 10 cc/min O_2 flow, 75 mtorr base pressure) and the channels rendered hydrophobic by coating with Aquapel (Pittsburgh Glass Works, LLC, Pittsburgh, PA). Each microfluidic device (Fig. 1(c), Fig. S1) contained two inlets, one for a fluorinated droplet generation oil (Bio-Rad, Hercules, CA) and the other for an aqueous suspension of fluorescent beads, used to form precursors to the hydrogel-based barcode particle. This aqueous suspension consisted of 10 μm diameter carboxylated fluorescent polystyrene beads with Ex/Em 488/509 nm

Optics EXPRESS

(Magsphere Inc., Pasadena, CA). These beads were purified by centrifugation and supernatant removal and resuspended in a mixture consisting of 6.5% v/v acrylamide (40% concentration), 9% v/v acrylamide/bis-acrylamide (40% solution, 19:1 feed ratio), 0.3% wt/vol ammonium persulfate, 15% v/v OptiPrep (Sigma-Aldrich, St. Louis, MO) and deionized water at concentrations ranging from 2.25×10^7 microspheres/mL to 7.88×10^7 microspheres/mL. The OptiPrep (density of 1.32 g/mL) allowed the mixture's density to match that of polystyrene, preventing unwanted sedimentation of the microspheres during the experiment. The negatively charged carboxylate surface functionalization reduced agglomeration of the beads. To help catalyze the cross-linking of the hydrogel, 0.4% v/v tetramethylethylenediamine (Sigma-Aldrich, St. Louis, MO) was added to the fluorinated oil. Flow of the droplet generation oil and microsphere mixture into the microfluidic device was controlled by a pressurized source coupled with a feedback flow controller (Fluigent, North Chelmsford, MA). Droplets ranging in diameter from 30 μm to 50 μm could be fabricated at rates in excess of 2.5 kHz at the flow focusing junction (cross section w x h = 40 μm x 50 μm). The process was monitored using a high-speed camera (Integrated Design Tools, Inc., Pasadena, CA). In a typical experiment, approximately 1 mL of the emulsion was collected in a polypropylene microcentrifuge tube. The emulsion was then incubated overnight in a 65 °C oven, forming cross-linked hydrogel microparticles in oil. The particle mixture was then washed by five rounds of centrifugation and resuspension in hexane (Sigma-Aldrich, St. Louis, MO). Finally, the particle mixture was filtered through a 20 μm strainer removing most of the hexane and any free microspheres released from hydrogel beads damaged during the washing steps. After filtering, barcode particles remaining on the strainer mesh were removed and resuspended in deionized water using a transfer pipette. To visualize the barcode particles, the suspension was wicked into a w x h = 1 mm x 0.1 mm rectangular glass capillary (VitroCom Inc. Mountain Lakes, NJ) and viewed using a widefield microscope (Keyence, Osaka, Japan).

2.2. Optical measurements

Barcode particles were read by measuring spectra emanating from their embedded microspheres. These microspheres were excited using a continuous-wave 491 nm laser (Hübner Photonics, Kassel, Germany) with a typical power of 180 μW focused to a 6 μm spot size by underfilling a 10x objective (Leica Microsystems, Wetzlar, Germany). Emission light was separated using a 505 nm cutoff dichroic mirror and a 500 nm longpass filter (Thorlabs, Newton, NJ). The light's spectrum was then recorded over a 10 ms exposure duration using a ~0.2 nm resolution grating-based spectrometer comprising of an electron multiplied charge coupled device (EMCCD) (Andor Technology, Belfast, United Kingdom), and calibrated using an Argon lamp (Newport Corporation, Irvine, CA). Figure 1(b) shows a typical measured spectrum of a fluorescent microsphere embedded in a hydrogel bead using this optical configuration. The polystyrene's refractive index $n_{ps} = 1.59$ is higher than that of the hydrogel $n_h = 1.35$ as measured by refractometer (Sper Scientific, Scottsdale, AZ), hence the presence of sharp WGM peaks arising from the microsphere's resonances. Since these peaks were spectrally separated by a wavelength greater than the resolution of the spectrometer, each was easily resolved. For barcoding, it was convenient to remove the fluorescence background of the emission by subtracting the convolution of the spectrum with a Gaussian filter. Peaks corresponding to WGM resonances were identified by custom code (MathWorks Inc., Natick, MA) allowing us to infer microsphere diameters.

3. Results and discussion

3.1. Barcode formation

By varying the flow conditions into the microfluidic chip, we were able to fabricate monodisperse droplets ranging from 30-50 μm in diameter. Attempts to form smaller droplets typically led to

Optics EXPRESS

high degrees of polydispersity since the encapsulated microspheres were comparable in size to the droplets and so disrupted their formation. By tuning this flow ratio, we were able to alter the size of the droplets produced, thereby altering the average number of microspheres, and thus constituent barcodes per bead (Fig. 2, Fig. S2). As expected, increasing the oil to aqueous flow ratio decreased droplet size [25]. Importantly, the achievable generation rate of barcoding particles was in excess of 2.5 kHz, making our method a viable technique for high throughput generation of barcodes (see Visualization 1).

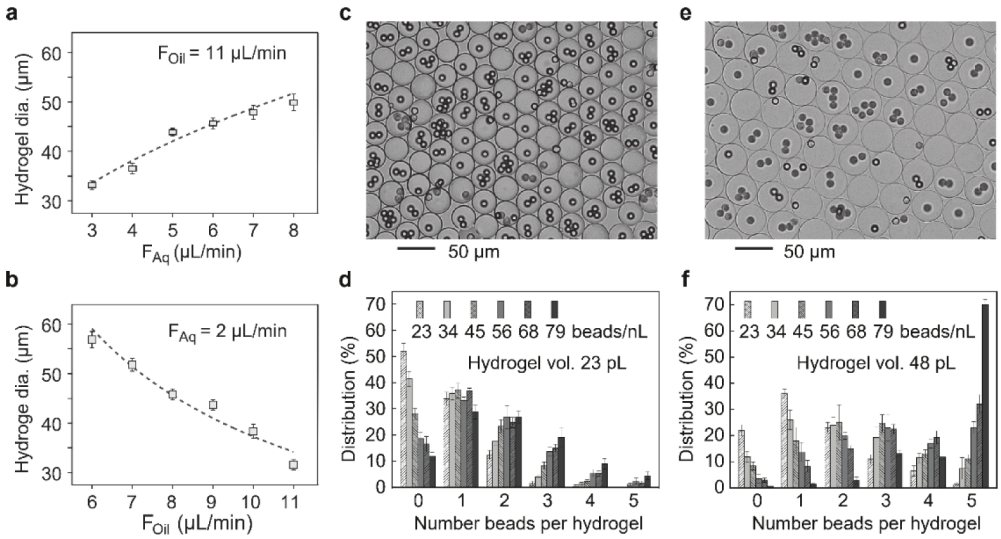

Fig. 2. Statistics of stochastic barcode fabrication. (a) Dependence of droplet size on the flow speed of the aqueous mixture. (b) Dependence of droplet size on the oil flow speed. (c) 35 μm diameter barcode particles. (d) Statistical distribution of microspheres per particle depending on initial microsphere concentrations within the aqueous mixture for 35 μm diameter barcode particles. (e) 45 μm diameter barcode particles. (f) The statistical distribution for particles of size 45 μm.

Any effective barcoding scheme must have enough diversity to generate large numbers of distinct barcodes. In our design, this occurs through a stochastic process in which beads of slightly different diameter are encapsulated and then fixed within the same droplet/barcode particle. By altering the size of the hydrogel particle through variation of the microfluidic flow conditions and the concentration of the microspheres within the aqueous mixture, we were able to tune the distribution of microspheres within each particle. For a ratio of lower than 3 beads per particle, we found the distribution was governed by the Poisson statistics with a mean given by the product of the microsphere concentration and droplet volume (Figs. 2d, f). However, for more than 3 beads per particle, the distribution deviated from Poisson statistics with a heightened probability of seeing large numbers of encapsulated microspheres. Likely, these events happened due to agglomeration of the microspheres before reaching the flow focusing junction.

3.2. Barcode measurements

Measurements of barcoding particles were performed by exciting the fluorescently doped microspheres using a 491 nm excitation laser and collecting the emission light using a grating-based spectrometer. The small cavity size and high refractive index of the polystyrene relative to the surrounding hydrogel trapped some of the emitted fluorescence within the microsphere. Certain discrete wavelengths within the spectrally broad (~30 nm full width at half maximum (FWHM)) fluorescence emission range, resonate within the periphery of the microsphere. These

Optics EXPRESS

wavelengths represent solutions to Maxwell's equations and its associated boundary conditions, which lead to the formation of a WGM pattern within the microsphere (Fig. 3(a)). These discrete solutions, known as cavity modes, can be referenced by a set of indexes [26]. The experimentally observed modes are all of first order in radial index but may each correspond to different polar indexes l and polarizations. They can therefore be described by TE_l and TM_l where TE and TM represent the different polarizations corresponding to a 0 radial electric field component and radial magnetic field component, respectively. The wavelength associated with each of these modes is determined by the cavity geometry, which, in the case of a sphere is described by the diameter. Figure 3(b) shows this dependence for a few select modes.

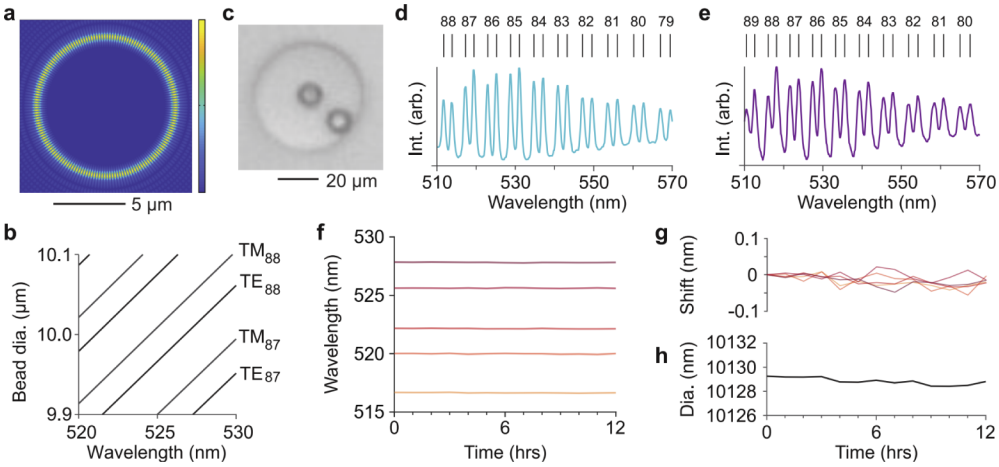

Fig. 3. Properties of hydrogel-embedded microsphere cavities. (a) The fundamental electric-field WGM pattern of the resonant mode TE_{84} in a microsphere with a diameter of 10 μm. (b) Relationship between microsphere diameter and wavelengths of the resonances. (c) Barcode particle containing two microspheres. (d) Normalized measured spectrum and polar index labelled resonant peak locations of the first microsphere of a barcode particle. (e) Spectrum of the second microsphere. (f) Resonant wavelengths of a microsphere within a hydrogel bead measured each hour over 12 hrs. (g) Shifts of these resonant wavelengths during this measurement. (h) Computed diameter from the resonances.

Experimentally, these resonances result in numerous resonance ~1 nm FWHM peaks, the locations of which can act as an identifiable signature. Figure 3(c) shows an exemplary hydrogel particle containing two microspheres. Its spectral signature is associated with the signature arising from *both* microspheres (Figs. 3d, e) resulting in combinatorial scaling of the signature's complexity. Though barcoding directly based on peak locations has previously been demonstrated [13,27], a further simplification is possible by using the relationship between peak location and microsphere size. In this case, only the diameter of each microsphere need be stored when keeping track of barcodes, which leads to a significant reduction in computational complexity. We translate the experimental measurement of resonant peak locations to diameter through a least-squares minimization fit. To decrease the computational time of translation, we obtained a direct relationship between peak locations and diameter based on the exact solution of Maxwell's equations for a dielectric sphere [26,28] of refractive index 1.59 embedded in an environment of refractive index 1.35 for l between 60 and 120 over a diameter range of 8 μm to 12 μm, in steps of 0.02 nm. This created a lookup table which was then interpolated using cubic polynomials during the minimization process. This strategy allowed us to rapidly compute a diameter barcode associated with each particle. For example, the barcode particle in Fig. 3(c) has two sets of resonant peaks: one corresponding to a diameter (D_1) of 9.751 μm (Fig. 3(d)) and the other

Optics EXPRESS

to a diameter (D_2) of 9.835 μm (Fig. 3(e)) and hence a barcode of (D_1, D_2) = (9.751, 9.835). Importantly, since the spatial positions of the beads are fixed within each particle, the assigned barcode will still be reliably retained over successive measurements. This is a distinct advantage over previous work in which objects, such as cells, have been spectrally barcoded by placing multiple beads within its interior. Since the bead locations are not fixed, their motion within the cells could lead to subtle spectral changes that are largely avoided in this work. Importantly, this barcode remains stable over time and repeated measurements. We note that the wavelength of the spectral peaks exhibiting the highest signal-to-noise ratio typically lies in the approximate range of 515 nm to 530 nm. These peaks are therefore ideal to fit to a diameter-based barcode. Figure 3(f) shows a time-lapse variation of modal peaks within this wavelength range of a single microsphere embedded within a hydrogel particle, measured each hour over a 12 hr period. Typically, each resonant peak shifted by less than 0.1 nm (Fig. 3(g)). These peak wavelength locations remained stable even when high excessive excitation laser power was used that resulted in significant intensity loss due to photobleaching (Fig. S3). By repeatedly fitting the diameter based on the resonant peak wavelengths, we determined that these slight shifts corresponded to an uncertainty in diameter, or the standard deviation, σ, of just 0.29 nm (Fig. 3(h)) about a mean diameter D of 10,128.84 nm. This corresponds to a relative diameter error of 3×10^{-5}.

To provide a simple, rough estimate of the stability required to adequately barcode particles we assume that this measurement uncertainty can be modelled by a normal distribution $N(D, \sigma^2)$. Then, the probability p_d that the measured barcodes of two particles with true diameters differed by d times the standard deviation (i.e. D and $D + d\sigma$) will be correctly assigned is given by $0.5(1 + |\mathrm{erf}(d/2)|)$ (Supplement 1). Since we intend to create an extremely large number of unique barcodes K (e.g. $> 10^6$), the spacing between diameter barcodes should be sufficiently large that despite this large number, only a small error occurs. Specifically, the worst-case probability that all barcodes are measured within d standard deviations of their true value is given as $(p_d)^{K-1}$ if we consider only nearest neighbor interactions. Thus, we pick p_8, which, in the case of $K = 10^6$ would lead to a 99.2% probability that all one million measured barcodes are correctly assigned.

3.3. Estimating barcode diversity

Twenty particles each containing one, two or three microspheres (termed singlets, doublets and triplets) were measured to estimate barcode diversity arising from our microfluidic fabrication technique. Each microsphere spectrum was mapped to a bead diameter. The distribution of diameters (a total of 120 microspheres) was roughly Gaussian (Fig. 4(a)) with a mean of 9.76 μm and a FWHM of 452 nm. Based on our uncertainty estimate, a simple metric for each barcode particle to be unambiguously identifiable, could be that each is separated by a distance greater than 8 σ, or 2.06 nm according to our earlier diameter uncertainty estimate (Fig. 3(h)). Therefore, for a singlet barcode particle to be uniquely identifiable with high probability, no other particle in the measurement set should have a diameter located within this surrounding uncertainty interval. For a singlet, since only a single diameter is associated with each barcode, the probability of overlap is significantly higher than in the doublet or triplet cases. This can be visualized by representing each barcode as a point in space, surrounded by a region representing the measurement uncertainty. In the singlet case, overlap is relatively more likely since each barcode lies along a line representing each microsphere's diameter (Fig. 4(b)). By contrast, a doublet, which is associated with two diameter barcodes lies in a segment of the plane (Fig. 4(c)). Note that since a doublet particle containing microspheres of diameter D_1 and D_2 is identical to another particle containing microspheres of diameter D_2 and D_1, each barcode is described by a location that exists only in half the area spanned by the two diameters. We have arbitrarily chosen to order the microsphere diameter barcodes in increasing order. For a triplet particle, which can be described as a location in a 3D space, the chance of overlap is even further reduced (Fig. 4(d)).

Optics EXPRESS

Note that this geometrical picture suggests the possibility of more complicated uniqueness analysis. For example, one could take each barcode, represented by a point in an m dimensional space for a multiplet consisting of m components, and model the barcode's stability over time as a convection-diffusion process. Incorrect barcoding would then occur when the distance metric separating pairs of barcodes becomes less than the uncertainty associated with each measurement. In other words, this measurement uncertainty is represented by a collision cross-section associated with each barcode, whose movement is governed by convection-diffusion.

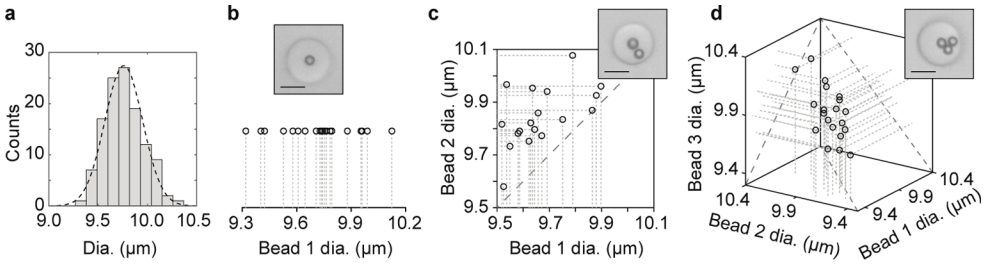

Fig. 4. The diversity of multiplet barcodes. (a) Histogram showing the fit diameters of 120 microspheres embedded in hydrogel. (b-d) Distribution of measured barcodes of multiplets consisting of one (b), two (c), or three (d) microspheres. Scale bar 30 μm.

Assuming a single microsphere can generate M uniquely identifiable barcodes, m microspheres embedded within a single bead can, according to the simple analysis conducted in previous studies [13,29], generate $N(m) = \frac{M!}{m!(M-m)!}$ barcodes. As a simple estimation, $M \approx \text{FWHM}/(\pm 8\,\sigma) = 110$. So, $N(1) = 110$, $N(2) = 5,995$, and $N(3) = 215,820$. Therefore, we see that as the span of possible microsphere diameters increases, so too does the number of unique barcodes. For a finite number N of unique barcodes, as the number, n, of samples to be tagged increases, the probability, P, of any individual sample having the same barcode as another sample, i.e. a duplicate error, increases. Theoretically, $P \approx \frac{n}{N}$ for $n<N$ (Supplement 1).

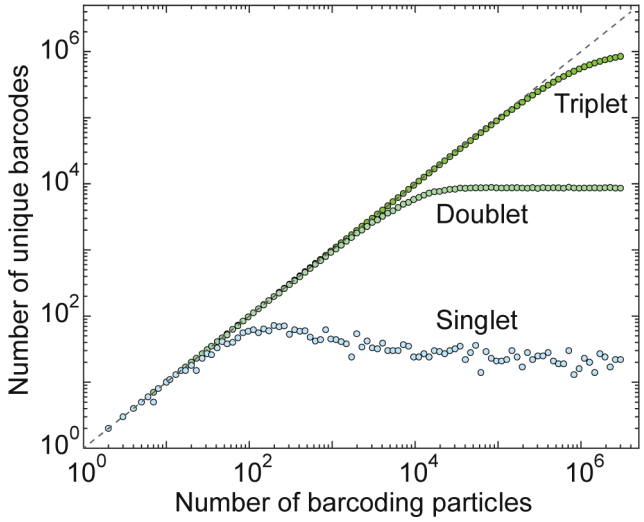

Fig. 5. Numerical simulation of unique barcodes as a function of the number of randomly produced particles. About 10^2, 10^4, and 10^6 unique barcodes can be generated using singlet, doublet, and triplet barcode schemes, respectively.

Optics EXPRESS

Next, we performed computer simulations to predict the actual number of unique barcodes formed in our real experiment accounting for the random distribution from which the barcodes are drawn (i.e. the distribution of microsphere diameters). Given a specific number of barcode particles n, we computed the expected number that were unique by randomly drawing diameters from the measured Gaussian distribution (Fig. 4(a)) for singlets, doublets, and triplets, respectively, assuming uniqueness was lost when any pair were separated by a distance less than 8 σ (Fig. 5). For singlets, the maximum number of unique barcodes is reached when about 200 particles are used, of which approximately 10^2 are unique. By contrast, doublets result in a maximum of approximately 10^4 unique barcodes, and triplets 10^6.

4. Conclusions

Here, we have presented the concept of a multiplet WGM-based barcode along with a high-throughput microfluidic technique to generate hundreds of thousands of unique microparticle barcodes in just a few minutes. At a droplet generation rate of 2.5 kHz, we estimate that our production technique created 100,000 unique barcodes in less than 3 min. Barcode particles were read by measuring the spectra of the constituent beads. Assuming a particle diameter of 30 μm, a bead diameter of 10 μm, and an exposure time of 10 ms, we can approximate this readout time as 10 ms x (30 μm /10 μm)^2 = 90 ms. It would therefore take at least 2.5 hr to read out 100,000 barcodes. Several future improvements are possible that could further enhance multiplexing and increase barcode readout speed. While we have used a single color of cavity bead in this work, it should be feasible to instead use beads each with different, ideally non-overlapping, emission spectra. High-speed readout of multiple microsphere barcodes could then be performed simultaneously without spectral overlap from different beads complicating any subsequent size fitting. Furthermore, while a goal of this research has been to compare the multiplexing abilities of multiplets consisting of different numbers of constituent barcodes, for some applications it might be advantageous for particles which have a high multiplexing ability to be isolated. In the case of microspheres doped with fluorescent molecules, this could be accomplished by using commercially available fluorescent-based flow sorting devices to pick out hydrogel beads with the desired number of embedded microspheres. Alternatively, multiplets with specific numbers of embedded microspheres could be generated during the microfluidic fabrication process by, for example, using inertial ordering of microspheres in the channel to accurately control the encapsulation process [30]. Alternatively, microfluidic devices could be used to create double emulsions [31,32] comprised of a specific number of inner droplets, encapsulated within an outer droplet. Each inner droplet would form a precursor to the resonator cavity, and each outer droplet would form the precursor to the encapsulating bead. This method would enable microparticle barcodes to each be comprised of a controllable, predetermined number of microspheres, thus avoiding the production of any unwanted (e.g., empty) particles. A further advantage would be that the randomization of microsphere diameters could be rationally designed through control of the flow rates.

We believe the type of particle demonstrated here could be used in multiplexing applications that require large numbers of unique barcodes. For example, some modern single-cell sequencing techniques use hundreds of thousands of nucleotide-based barcodes, coupled to hydrogel beads, to tag genetic material from different cells [33]. By linking these nucleotide-based barcodes to the optical barcodes we have shown here, would result in the formation of an optically readable genetic tag [34]. In the future, even smaller multiplet microparticle barcodes could be produced by using 2-3 μm diameter embedded resonators of higher refractive index material [20,21,35]. Since flow focusing microfluidics can generate monodisperse droplets as small as 900 nm [36], our general microfluidic approach could be used to fabricate even smaller multiplet particles. These particles could be suitable for tagging individual eukaryotic cells by introducing each particle into the cell cytoplasm. Importantly, since each resonator would be encapsulated as part

Optics EXPRESS

of an indivisible composite particle, such a barcode could be used to track cells across multiple generations of cell divisions whilst retaining its unique spectral signature.

Funding. Massachusetts General Hospital; National Institutes of Health (DP1-OD022296, P41-EB015903); China Scholarship Council; Optical Society; National Science Foundation (ECCS-2025158).

Disclosures. P.H.D. and S.H.Y. hold patents on technologies related to the devices developed in this work. S.H.Y. has financial interests in LASE Innovation Inc., a company focused on commercializing technologies based on optical barcodes, that were reviewed and are managed by Massachusetts General Hospital and Partners HealthCare in accordance with their conflict-of-interest policies.

Data availability. Data underlying the results presented in this paper are not publicly available at this time but may be obtained from the authors upon reasonable request.

Supplemental document. See Supplement 1 for supporting content.

References

1. A. R. Vaino and K. D. Janda, "Euclidean shape-encoded combinatorial chemical libraries," Proc. Natl. Acad. Sci. U. S. A. **97**(14), 7692–7696 (2000).
2. Y. Li, Y. T. H. Cu, and D. Luo, "Multiplexed detection of pathogen DNA with DNA-based fluorescence nanobarcodes," Nat. Biotechnol. **23**(7), 885–889 (2005).
3. S. A. Dunbar, "Applications of Luminex® xMAP^{TM} technology for rapid, high-throughput multiplexed nucleic acid detection," Clin. Chim. Acta **363**(1-2), 71–82 (2006).
4. B. D. Tait, F. Hudson, L. Cantwell, G. Brewin, R. Holdsworth, G. Bennett, and M. Jose, "Review article: Luminex technology for HLA antibody detection in organ transplantation," Nephrology **14**(2), 247–254 (2009).
5. J. Lee, P. W. Bisso, R. L. Srinivas, J. J. Kim, A. J. Swiston, and P. S. Doyle, "Universal process-inert encoding architecture for polymer microparticles," Nat. Mater. **13**(5), 524–529 (2014).
6. S. Matthias, J. Schilling, K. Nielsch, F. Müller, R. B. Wehrspohn, and U. Gösele, "Monodisperse diameter-modulated gold microwires," Adv. Mater. **14**(22), 1618–1621 (2002).
7. D. Dendukuri, D. C. Pregibon, J. Collins, T. A. Hatton, and P. S. Doyle, "Continuous-flow lithography for high-throughput microparticle synthesis," Nat. Mater. **5**(5), 365–369 (2006).
8. D. C. Pregibon, M. Toner, and P. S. Doyle, "Multifunctional Encoded Particles for High-Throughput Biomolecule Analysis," Science **315**(5817), 1393–1396 (2007).
9. E. Fernandez-Rosas, R. Gómez, E. Ibañez, L. Barrios, M. Duch, J. Esteve, C. Nogués, and J. A. Plaza, "Intracellular Polysilicon Barcodes for Cell Tracking," Small **5**(21), 2433–2439 (2009).
10. S. A. Dunbar and M. R. Hoffmeyer, "CHAPTER 2.9 - Microsphere-Based Multiplex Immunoassays: Development and Applications Using Luminex® xMAP® Technology," Immunoass. Handb., 157–174 (2013).
11. M. Foreman, J. Swaim, and F. Vollmer, "Whispering gallery mode sensors," Adv. Opt. Photonics **7**(2), 168–240 (2015).
12. D. Richter, M. Marinčič, and M. Humar, "Optical-resonance-assisted generation of super monodisperse microdroplets and microbeads with nanometer precision," Lab Chip **20**(4), 734–740 (2020).
13. M. Humar and S. H. Yun, "Intracellular microlasers," Nat. Photonics **9**(9), 572–576 (2015).
14. M. Schubert, A. Steude, P. Liehm, N. M. Kronenberg, M. Karl, E. C. Campbell, S. J. Powis, and M. C. Gather, "Lasing within Live Cells Containing Intracellular Optical Microresonators for Barcode-Type Cell Tagging and Tracking," Nano Lett. **15**(8), 5647–5652 (2015).
15. H. Zhang, P. Palit, Y. Liu, S. Vaziri, and Y. Sun, "Reconfigurable Integrated Optofluidic Droplet Laser Arrays," ACS Appl. Mater. Interfaces **12**(24), 26936–26942 (2020).
16. A. Bamshad and H. J. Cho, "Laserjet Printed Micro/Nano Sensors and Microfluidic Systems: A Simple and Facile Digital Platform for Inexpensive, Flexible, and Low-Volume Devices," Adv. Mater. Technol., 2100401 (2021).
17. H. Zhang, C. Zhang, S. Vaziri, F. Kenarangi, and Y. Sun, "Microfluidic Ionic Liquid Dye Laser," IEEE Photonics J. **13**(1), 1 (2021).
18. L. Zheng, M. Zhi, Y. Chan, and S. A. Khan, "Embedding liquid lasers within or around aqueous microfluidic droplets," Lab Chip **18**(1), 197–205 (2018).
19. I. M. Kennedy, M. Tanyeri, and R. Perron, "Lasing droplets in a microfabricated channel," Opt. Lett. **32**(17), 2529–2531 (2007).
20. N. Martino, S. J. J. Kwok, A. C. Liapis, S. Forward, H. Jang, H.-M. Kim, S. J. Wu, J. Wu, P. H. Dannenberg, S.-J. Jang, Y.-H. Lee, and S.-H. Yun, "Wavelength-encoded laser particles for massively multiplexed cell tagging," Nat. Photonics **13**(10), 720–727 (2019).
21. A. H. Fikouras, M. Schubert, M. Karl, J. D. Kumar, S. J. Powis, A. Di Falco, and M. C. Gather, "Non-obstructive intracellular nanolasers," Nat. Commun. **9**(1), 4817 (2018).
22. C. Feng, Z. Xu, X. Wang, H. Yang, L. Zheng, and H. Fu, "Organic-Nanowire-SiO2 Core-Shell Microlasers with Highly Polarized and Narrow Emissions for Biological Imaging," ACS Appl. Mater. Interfaces **9**(8), 7385–7391 (2017).
23. R. Zilionis, J. Nainys, A. Veres, V. Savova, D. Zemmour, A. M. Klein, and L. Mazutis, "Single-cell barcoding and sequencing using droplet microfluidics," Nat. Protoc. **12**(1), 44–73 (2016).

Optics EXPRESS

24. E. Z. Macosko, A. Basu, A. Regev, S. A. Mccarroll, E. Z. Macosko, A. Basu, R. Satija, J. Nemesh, K. Shekhar, and M. Goldman, "Highly Parallel Genome-wide Expression Profiling of Individual Cells Using Nanoliter Droplets Resource Highly Parallel Genome-wide Expression Profiling of Individual Cells Using Nanoliter Droplets," Cell **161**(5), 1202–1214 (2015).
25. S. L. Anna, N. Bontoux, and H. A. Stone, "Formation of dispersions using "flow focusing" in microchannels," Appl. Phys. Lett. **82**(3), 364–366 (2003).
26. S. Balac, "WGMode: A Matlab toolbox for whispering gallery modes volume computation in spherical optical micro-resonators," Comput. Phys. Commun. **243**(1), 121–134 (2019).
27. M. Humar, A. Upadhya, and S. H. Yun, "Spectral reading of optical resonance-encoded cells in microfluidics," Lab Chip **17**(16), 2777–2784 (2017).
28. A. N. Oraevskij, "Whispering-gallery waves," Quantum Electron. **32**(5), 377–400 (2002).
29. S. J. J. Kwok, N. Martino, P. H. Dannenberg, and S. H. Yun, "Multiplexed laser particles for spatially resolved single-cell analysis," Light: Sci. Appl. **8**(1), 74 (2019).
30. D. Di Carlo, D. Irimia, R. G. Tompkins, and M. Toner, "Continuous inertial focusing, ordering, and separation of particles in microchannels," Proc. Natl. Acad. Sci. **104**(48), 18892–18897 (2007).
31. S. H. Kim, J. W. Shim, and S. M. Yang, "Microfluidic multicolor encoding of microspheres with nanoscopic surface complexity for multiplex immunoassays," Angew. Chem., Int. Ed. **50**(5), 1171–1174 (2011).
32. Shingo Okushima, Takasi Nisisako, Toru Torii, and T. Higuchi, "Controlled Production of Monodisperse Double Emulsions by Two-Step Droplet Breakup in Microfluidic Devices," Langmuir **20**(23), 9905–9908 (2004).
33. A. M. Klein, L. Mazutis, D. A. Weitz, M. W. Kirschner, A. M. Klein, L. Mazutis, I. Akartuna, N. Tallapragada, A. Veres, V. Li, and L. Peshkin, "Droplet Barcoding for Single-Cell Transcriptomics Applied to Embryonic Stem Cells Resource Droplet Barcoding for Single-Cell Transcriptomics Applied to Embryonic Stem Cells," Cell **161**(5), 1187–1201 (2015).
34. S.-H. Yun and P. H. Dannenberg, "Multiplexed Single-Cell Analysis Using Optically-Encoded RNA Capture Particles," U.S. patent WO 2020/086510 A1 (2020).
35. K. Kim, P. H. Dannenberg, H. Yan, S. Cho, and S. Yun, "Compact Quantum-Dot Microbeads with Sub-Nanometer Emission Linewidth," Adv. Funct. Mater., **2103413**, 1 (2021).
36. F. Malloggi, N. Pannacci, ele Attia, F. Monti, P. Mary, H. Willaime, P. Tabeling, B. Cabane, and P. Poncet, "Monodisperse Colloids Synthesized with Nanofluidic Technology," Langmuir **26**(4), 2369–2373 (2010).

Supplemental Document

Optics EXPRESS

Droplet microfluidic generation of a million optical microparticle barcodes: supplement

PAUL H. DANNENBERG,[1,2,4] JIE WANG,[1,3,4] YUE ZHUO,[1] SANGYEON CHO,[1] KWON-HYEON KIM,[1] AND SEOK-HYUN YUN[1,2,*]

[1] *Harvard Medical School and Wellman Center for Photomedicine, Massachusetts General Hospital, Boston, Massachusetts 02114, USA*
[2] *Harvard-MIT Health Sciences and Technology, Massachusetts Institute of Technology, Cambridge, Massachusetts 02139, USA*
[3] *College of Artificial Intelligence, Nanjing Agricultural University, Nanjing 210031, China*
[4] *Co-first authors with equal contribution.*
[*] *syun@hms.harvard.edu*

Supplement DOI: https://doi.org/10.6084/m9.figshare.16578005

Parent Article DOI: https://doi.org/10.1364/OE.439143

Droplet microfluidic generation of a million optical microparticle barcodes: supplemental document

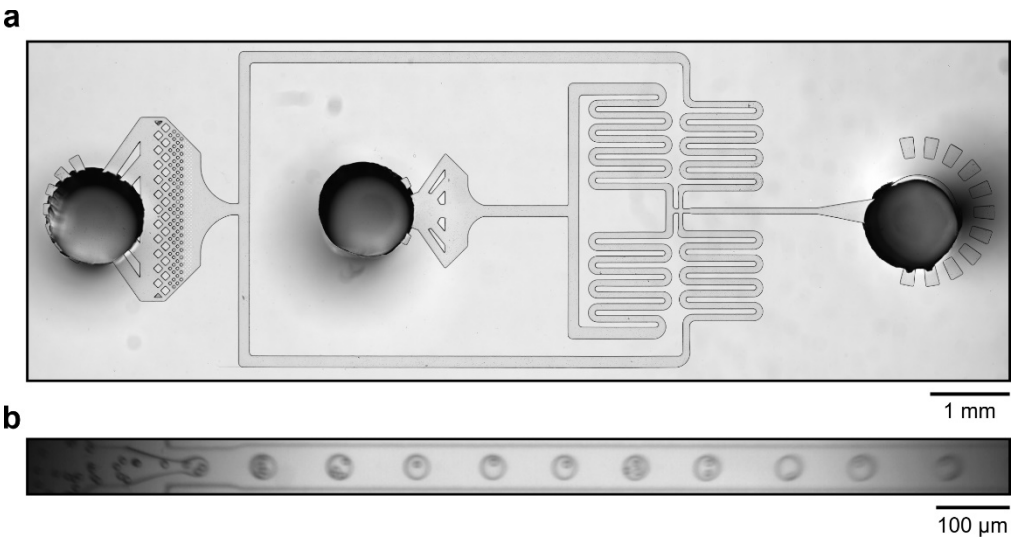

Fig. S1. Droplet generation microfluidic device. (a) Brightfield image of the droplet generation device. The leftmost punched hole is the oil inlet, the centermost hole the aqueous inlet and the rightmost punched hole the droplet outlet. (b) Image of droplets being formed at the junction, taken using a high-speed camera (8 µs exposure duration) at an oil:aqueous flow ratio of 6:1.

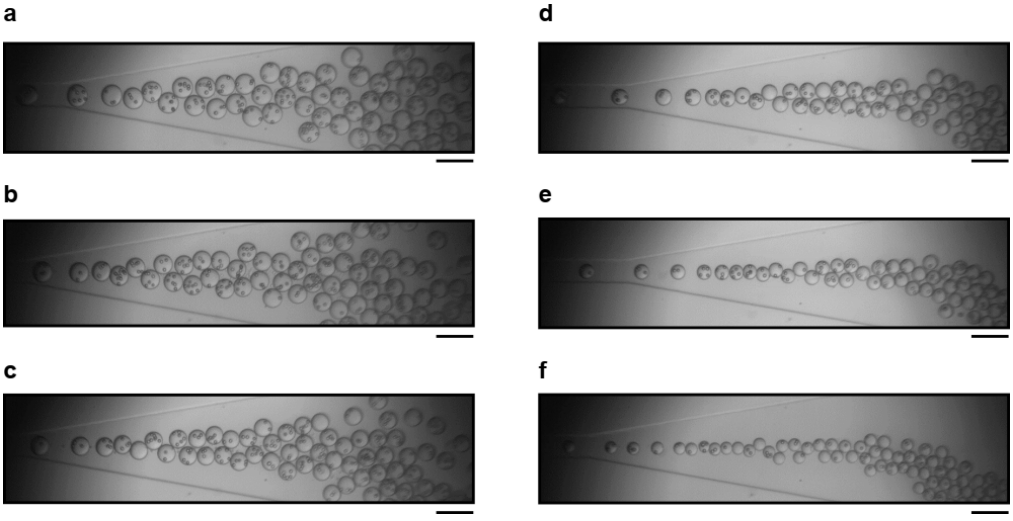

Fig. S2. Droplet/barcode particle size control. Brightfield images downstream of the flow focusing junction taken during microfluidic device operation at an aqueous flow of 2 µL/min and an oil flow of (a) 6 µL/min (b) 7 µL/min (c) 8 µL/min (d) 9 µL/min (e) 10 µL/min (f) 11 µL/min. Scalebar 100 µm.

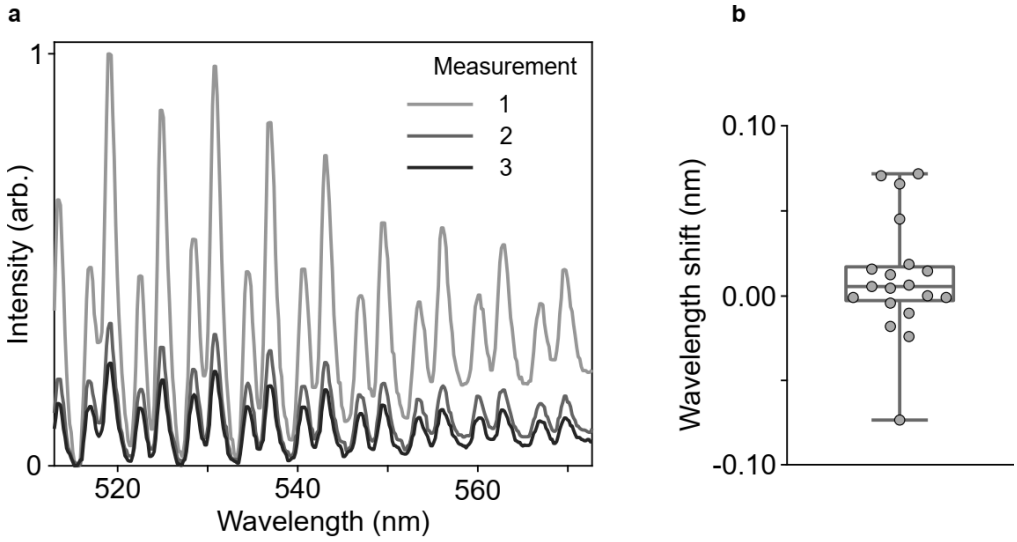

Fig. S3. WGM peak stability during photobleaching. (a) WGM spectra of a fluorescently doped polystyrene microsphere as it is photobleached by high power laser. Measurement 1 corresponds to the initial measurement, measurement 2 is taken after 30 seconds of photobleaching and measurement 3 is taken after another 30 seconds of photobleaching. (b) Peak wavelength shift between measurement 1 and measurement 3.

Note 1: Error probability of two barcodes

Consider two barcode particles. In the simplest case, each barcode can be described by a single diameter. Assume the first true barcode diameter is D_1 and the second D_2 with $D_2 > D_1$. Furthermore, we assume that each measurement of the barcode results in a normally distributed error $\varphi(x) = \frac{1}{\sigma\sqrt{2\pi}} e^{-x^2/2\sigma^2}$ where σ, the measurement uncertainty is specific to the barcoding system. Therefore, the probability that a particle's measured barcode is between D and $D + dD$ is $\varphi(D - D_1)$ and $\varphi(D - D_2)$ respectively for the first and second particles where dD is the differential element. Consider the scenario in which the first particle's barcode is measured to be D. Then we state that a barcoding error has occurred if the measured barcode of the second particle is less than D (i.e. the measured barcode of the second particle is closer to the true barcode of the first particle than the measured barcode of the first particle). Given the barcode measurement of the first particle was D, the probability of an error occurring is then $\int_{-\infty}^{D} \varphi(D' - D_2)\, dD'$. Accounting for all possible values D that can be measured for the first particle, the probability of a barcoding error P_E occurring is then

$$P_E = \int_{-\infty}^{\infty} \varphi(D - D_1) \int_{-\infty}^{D} \varphi(D' - D_2)\, dD' dD$$
$$= \int_{-\infty}^{\infty} \varphi(D - D_1)\, \Phi(D - D_2)\, dD,$$

where we have defined the cumulative distribution function $\Phi(x) = \int_{-\infty}^{x} \varphi(x')\, dx'$.To further simplify this expression, consider the partial derivative of P_E with respect to D_2

$$\begin{aligned}
\frac{\partial P_E}{\partial D_2} &= -\int_{-\infty}^{\infty} \varphi(D - D_1)\, \varphi(D - D_2)\, dD \\
&= -\frac{1}{2\pi\sigma^2} \int_{-\infty}^{\infty} \exp\left(-\frac{1}{2\sigma^2}\left[(D - D_1)^2 + (D - D_2)^2\right]\right) dD \\
&= -\frac{1}{\sqrt{2}\sigma\sqrt{2\pi}} \exp\left(-\frac{1}{2\sigma^2}\left(\frac{D_2 - D_1}{\sqrt{2}}\right)^2\right) \\
&\times \int_{-\infty}^{\infty} \frac{1}{\frac{\sigma}{\sqrt{2}}\sqrt{2\pi}} \exp\left(-\frac{1}{2\left(\frac{\sigma}{\sqrt{2}}\right)^2}\left(D - D_2 + \frac{1}{2}(D_2 - D_1)\right)^2\right) dD \\
&= -\frac{1}{\sqrt{2}}\varphi\left(\frac{D_2 - D_1}{\sqrt{2}}\right)
\end{aligned}$$

To compute P_E we simply integrate this expression

$$\begin{aligned}
P_E &= \frac{1}{\sqrt{2}} \int_{D_2}^{\infty} \varphi\left(\frac{D_2' - D_1}{\sqrt{2}}\right) dD_2' \\
&= 1 - \Phi\left(\frac{D_2 - D_1}{\sqrt{2}}\right) \\
&= \frac{1}{2}\left(1 - \mathrm{erf}\left(\frac{d}{2}\right)\right)
\end{aligned}$$

where in the final step we have written the cumulative distribution function in terms of the error function and defined $d = \frac{D_2 - D_1}{\sigma}$ as the distance between the two particle barcodes in units of the standard deviation of the measurement uncertainty.

Note 2: Duplication error

Consider there are an infinite number of barcoded particles with N different types (unique ID's) in a pool. And, we are taking out n particles from the pool in order to tag n samples. We are interested in calculating how many samples would have identical barcodes. When $n \ll N$, the most likely error is having a duplicate error: that is, two samples have the same barcode. The chance of having higher order errors, such as three samples having the same barcode, is relatively negligible. For each specific sample, the probability of it sharing an identical barcode with any one of the other samples, regardless of whether and how many of the other samples have their own duplicates or not, is given by:

$$P = (n - 1)\frac{(N - 1)^{n-2}}{N^{n-1}}$$

When $n \gg 1$ using $\lim_{N\to\infty}\left(1+\frac{1}{N}\right)^{N} = e$, we get

$$\lim_{N\to\infty} P = \frac{n}{N}e^{-\frac{n}{N}} \approx \frac{n}{N}$$

Visualization 1

Visualization 1 shows droplet generation at an oil:aqueous flow ratio of 6:1. The original video was captured using a high-speed camera operating at 7,280 frames per second. The video was then played at a speed of 20 fps (i.e., reduced in speed by a factor of 364).